ISSN 0025-6544, Mechanics of Solids, 2024, Vol. 59, No. 4, pp. 1–16. © Pleiades Publishing, Ltd., 2024.
Russian Text © The Author(s), 2024, published in Izvestiya Rossiiskoi Akademii Nauk, Mekhanika Tverdogo Tela, 2024, No. 4, pp. 00000–00000.

Mechanical Performances of Honeycomb Structures Reinforced by a Magnetorheological Elastomer Material: Experimental and Numerical Approaches

T. Djedid[a,*], A. Nour[a], S. Aguib[a,], N. Chikh[a,b], A.T. Settet[a], A. Khebli[c], L. Kobzili[a], Boudjana Abderzak[d], and M. Tourab[e]**

[a] *M'Hamed Bougara Boumerdes University, Motor Dynamics and Vibroacoustics Laboratory, Boumerdès, 35000 Algeria*

[b] *Mohamed El Bachir El Ibrahimi Bordj Bou Arreridj University, El-Anasser, 34030 Algeria*

[c] *M'Hamed Bougara Boumerdes University, Electrification of Industrial Enterprises Laboratory, Boumerdès, 35000 Algeria*

[d] *Industrial Technology Research Center, BP 64, Cheraga, Algeria, 16014 Algeria*

[e] *Badji Mokhtar Annaba University, Research Laboratory for Advanced Technologies in Mechanical Production, Annaba, 23000 Algeria*

**e-mail: t.djedid@univ-boumerdes.dz*

***e-mail:s.aguib@univ-boumerdes.dz*

Received June 8, 2024; revised September 19, 2024; accepted September 19, 2024

Abstract—In this article, the performance of mechanical resistance against failure of mechanical structures under bending load was studied by the use of a hybrid sandwich composite (Magnetorheological Elastomer (MRE) - Honeycomb). Accordingly, a series of four-point bending mechanical tests were carried out. In addition, a comparison of the force-deflection responses, the values of the maximum forces supported by each sample before damage were determined. Through the additional effect of the MRE core, the hybrid sandwich composite samples presented the best performances in terms of energy absorption-dissipation, and thanks to the effect of the honeycomb part, the Hybrid sandwich composite samples presented the best performance in terms of mechanical strength. To validate the performance of these developed hybrid structures, the numerical results are compared with the corresponding experimental results.

Keywords: Hybrid sandwich beam, Performance of mechanical resistance, MRE, Experimental analysis, Numerical simulation

DOI: 10.1134/S0025654424604221

1. INTRODUCTION

The development of smart composite materials in magnetorheological elastomer (MRE) continues to grow in the industry due to their advantages of controlling vibrations in real time and adapting to different external aggressions. Several works have been carried out in this area. Jamal et al. [1] realized an experimental, analytical and numerical study on composite facing multi-layer sandwich panels with polypropylene honeycomb core. A four-point bending test on a polypropylene honeycomb multi-layer sandwich panel were done by experimental investigations and the sandwich panel is homogenized and modelled using analytical and finite element methods to compute the four-point bending behavior. Anil al. [2] covered a literature review on magnetorheological elastomers manufacturing and characterizition. These materials are classified among the smart materials which are very influenced by the application of an external magnetic field, and then, their magneto-mechanical properties (moduli, stiffness, damping, ...) are sensitive and variable according to this external load. This makes magnetorheological (MR) materials very useful in different engineering domains. Fevzi et al. [3] proposed a new active control structure in order to suppress the vibrations of a wind turbine blade of small scale, made of extruded aluminum. They considered an SH3055 airfoil profile an interaction model of the magnetorheological patch and the electromagnetic actuator. Experimental investigations have been done and the results showed that the mag-

netorheological component of the structure can attenuate or suppress the blade vibrations. Bornassi et al. [4] studied turbomachinary blades made of sandwich composite material with embedded MRE core. They evaluated the interaction of bending-torsion effects on the futter stability boundaries using a classical sandwich tapered beam theory. Luca et al. [5], have concentrated on the study of the production and mechanical characterization of hybrid sandwich panels using hemp bi-grid cores that were manufactured with an ad hoc continuous manufacturing process. Sanjay et al. [6] studied the nonlinear characteristics of a simply supported moving system by the analytic-numeric approach under the joint influence of parametric and internal resonance. Miguel et al. [7] studied the influence of magnetic boundary conditions on magneto-mechanical models and demonstrated their importance to be considered in modelling strategy of the behavior modelling of these latters. They implemented a magneto-mechanical framework in the aim to evaluate the response of soft- and hard-magnetic MRE with application of uniform magnetic field. Hou et al. [8, 9] studied a range of experimental and numerical investigations on the mechanical behaviour of hexagonal honeycomb structures. They showed a significant influence of the magnetic field on the stiffness, the natural frequencies and the damping ratios of the beam. Mohammed et al. [10] investigated the magnetorheological-based sandwich beam subjected to free vibration and magnetoelastic loads. They used Hamilton principle to derive the structural governing equations and they solved the problem by finite element method and they compared their results with literature works. They showed that the magnetic field intensity and beam geometry influence largely the loss factor and deviate the first natural frequency. Guenfoud et al. [11] studied the mechanical behavior of hybrid honeycomb magnetorheological elastomer sandwich beams using an experimental and numerical approach. Umer et al. [12] simulated in Ansys a sandwich beam with honeycomb core filled of magnetorheological elastomer for various ratios of elastomer and iron particles. They showed the influence of the iron particles ratio on the different static and modal characteristis. The work realised by Felipe et al. [13] deals with the manufacturing and testing of sandwich beams with carbon/epoxy composite skins and a honeycomb core filled with magnetorheological elastomer (MRE) in different proportions of magneto/elastomer. Tourab et al. [14] experimentally studied the thermal effect of the magneto-mechanical behavior of elastomer; the latter is infilled with 25% of ferromagnetic particles of micrometric size; developed under the action of a magnetic field. The characterization of the rheological properties and the interaction between the micron size ferromagnetic particles as a function of the intensity of the magnetic field has been studied under the effect of different temperatures. Zniker et al. [15] studied the mechanical response and failure modes of two kinds of composite materials with PVC core and glass-fiber reinforced epoxy laminated composite under bending loading. To increase the efficiency of the pipeline repair system, Sharma et al. [16] focused on studying the characterization of the effect of using nano-silica in glass fiber reinforced polymer composite wrap. Modeling the failure of composite materials made of piezoelectric-magnetorheological elastomer layers constituting an active-passive damper has been done by Liu et al. [17]. They proposed a new method for evaluating the effect of the magnetic field on the structure rupture mechanism. Settet et al. [18] studied the three-point bending of a magnetorheological elastomer beam.

The bibliographic synthesis highlighted the interest in magnetorheological elastomer composites and the performances in terms of energy dissipation-absorption, the studies identified remain insufficient in terms of the coupling of mechanical resistance performance and energy dissipation-absorption.

The present work, of an experimental and numerical nature, aims to study the integration of a single or double magnetorheological elastomer core in a honeycomb structure to reduce the problem of failure through the absorption and dissipation of energy and increasing mechanical strength at the same time.

2. ANALYTICAL STUDY

An indirect method of measuring the properties of the core by sandwich bending allows to obtain a good evaluation of the shear modulus of the core with a four-point bending test as presented in Fig. 1.

The shear deformation theory proposed by Timoshenko [19]; was used to demonstrate the loading/deflection behavior of composite sandwich panels whose total deflection is the sum of bending and shear deformations. The shear stiffness of the core is relatively low compared to that of the skin, and usually results in significant shear deformation which should be taken into account in the total deflection of sandwich beam [1], [20].

$$w = w_b + w_s \tag{2.1}$$

where w, w_b and w_s are respectively the total deflection, the bending deflection and the shear deflection.

For a beam simply supported in static 4-point bending with an applied load P and a distance shear span a, the mid-span deflection of the beam is calculated by integrating the deflection between the support and

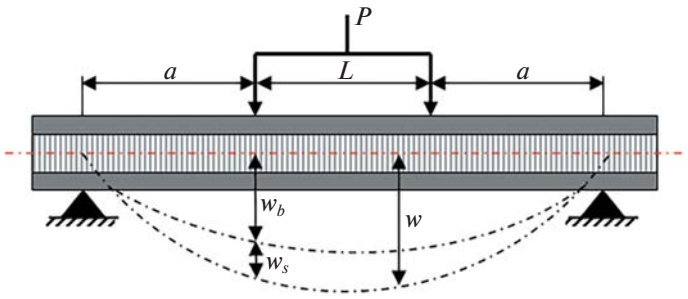

Fig. 1. Four-point bending of a sandwich beam.

the loading point ($0 < a < x$) and from the loading point to the mid-span $\left(0 < x < \frac{L}{2}\right)$, this relationship can be written as

$$w_b = 2\left[\int_0^a \left(\frac{M_L}{EI}\frac{x}{a}\right)\frac{x}{2}dx + \int_a^{\frac{L}{2}} \frac{M_L}{EI}\frac{x}{2}dx\right] \tag{2.2}$$

where EI is the bending stiffness of the cross section of the beam. In Eq. (2.2), M_L is common for both terms which allows us to simplify the equation as follows

$$w_b = \frac{M_L}{EI}\left[\int_0^a \left(\frac{x^2}{a}\right)dx + \int_a^{\frac{L}{2}} xdx\right] \tag{2.3}$$

For a simply supported beam, the shear displacement diagram is identical to the bending moment diagram, with a factor k/AG applied to it, with AG often called equivalent shear stiffness of sandwich beams [16] and k the shear correction factor [21]. The maximum bending moment occurs at the mid-span of the beam. Therefore, the shear strain at this location is then calculated as follows

$$w_s = \frac{k}{2AG}\int_0^a Pdx \tag{2.4}$$

For our case, $a = \frac{L}{3}$ and k, the shear correction factor $k = 1$.

3. EXPERIMENTAL ANALYSIS

3.1. Magnetorheological elastomer preparation

The elastomer (Fig. 2) is prepared by the following steps:

1- the silicone oil and the RTV141A polymer are put in a container and manual mixing is carried out for 15 minutes to obtain an elastomer in the form of a gel with good homogenization. A second container containing a quantity of iron particles of micrometric size to infill the elastomer is prepared.

2- a quantity of this gel obtained formed of silicone and RTV141A is mixed for 30 minutes with a quantity of iron particles until a homogeneous paw is obtained. By this process, an elastomer infilled with 30% of ferromagnetic particles was developed.

3- The leg obtained is degassed under vacuum for 10 minutes, in order to eliminate the air bubbles infiltrated during the mixing, to have a healthy structure for the experiment. The elastomer obtained is hermetically preserved at low temperature.

The quantities of the ingredients of the isotropic elastomer infilled with 30% of ferromagnetic particles of its total volume, are given in Table 1.

In order to obtain a magnetorheological elastomer, a sliding aluminum mold of rectangular shape 50 mm long, 20 mm wide and 4mm thick is manufactured. The elastomer paste, the preparation of which

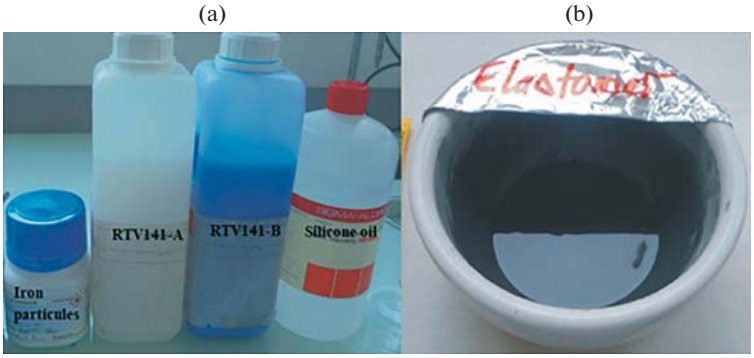

Fig. 2. Isotropic elastomer preparation, a) Ingredients b) Elastomer paste.

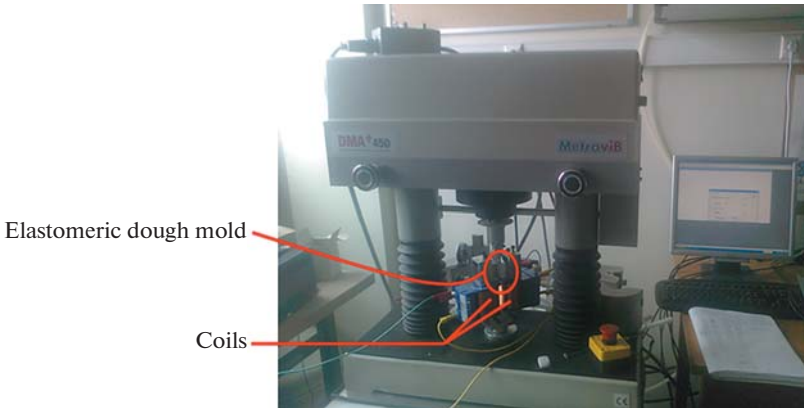

Fig. 3. Viscoanalyseur MetraviB DMA+ 450.

is described above, is injected so as to contain the volume of the mould. The mold containing the elastomer paste is placed in the MetraviB DMA+ 450 Viscoanalyzer and subjected to a variable magnetic field generated by the two coils (Fig. 3) to act on the alignment of the ferromagnetic particles.

The mechanical characteristics obtained are given in Table 2.

3.2. Elaboration and geometry of Honeycomb

The chosen honeycomb geometry is based on regular hexagonal cells Fig. 4.

The geometric parameters and mechanical properties of an aluminum honeycomb cell are presented in Table 3.

3.3. Elaboration of sandwich beams in magnetorheological elastomer honeycomb

In order to study the effect of the magnetorheological elastomer and the honeycomb on the mechanical resistance and the damping of the beam, we prepared four different specimens. The first specimen presents a magnetorheological elastomer beam (No. 1), the second presents a honeycomb beam (No. 2), the third presents a hybrid magnetorheological elastomer – honeycomb beam with a single layer of MRE

Table 1. Constituents of the elastomer infilled with 30% ferromagnetic particles

Time to crosslinking in hours	msilicone oil (g)	mRTV(A) (g)	mFe (g)	mRTV(B) (g)
24	1.064g	1.0385g	7.559	0.104

Table 2. Experimental data of DMA – $f = 100$ Hz

Shear strain	Storage modulus G' (Pa)	Dissipative modulus G'' (Pa)	Loss factor
$B = 0$ T			
0.00192032	1832829.12	432364.589	0.23590011
0.00144875	1284667.78	314776.282	0.24502544
0.00973429	1016428.99	249581.645	0.24554755
0.01952960	818620.224	220044.845	0.26879967
0.04856240	680515.968	189552.749	0.27854269
$B = 0.3$ T			
0.00475383	2965982.78	724816.704	0.24437657
0.00726697	2580620.54	633542.784	0.24550017
0.00969859	2313459.07	576327.398	0.24911934
0.01908080	1703498.11	463652.467	0.27217668
0.03362950	1316022.91	359488.896	0.27316310

Table 3. Geometric parameters and mechanical properties of the honeycomb cell

φ, mm	a, mm	b, mm	h, mm	t, mm	t', mm	q
6.35	3.66	3.66	5	1	2	30°

ρ_h, Kg/m^3	E_h, MPa	ν_h
2800	72000	0.33

(No. 3), and the last presents a hybrid magnetorheological elastomer – honeycomb beam with a double layer of MRE (No. 4), Fig. 5.

The tests are carried out on a universal hydraulic testing machine of the MTS compression-traction type, fitted with a 10 kN and 20 kN load cell for measuring the force and an LVDT sensor for measuring the displacement (Fig. 6), controlled and acquired by computer. The prepared hybrid sandwich beams (Fig. 5) are characterized by the four-point bending test (ASTM C1018 method [22]). The tests are carried out with a displacement speed of 2 mm/min.

The rupture of the sandwich beam clearly occurs upon gradually increasing the applied bending load. This rupture is mainly caused by the delamination between the aluminum skins and the honeycomb body, Fig. 7.

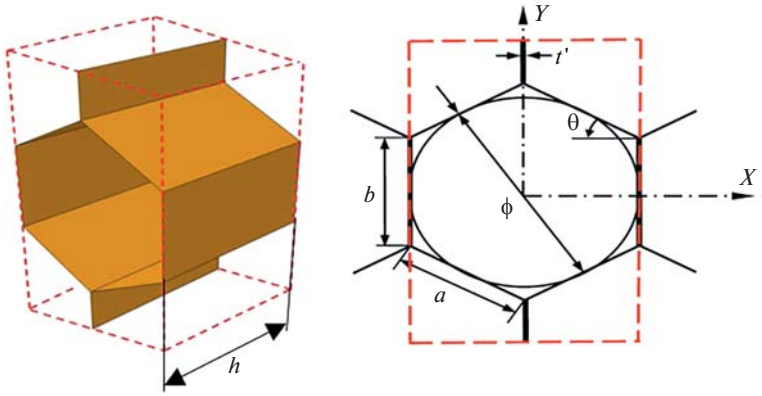

Fig. 4. Representative elementary volume and geometry of a honeycomb.

Fig. 5. Different prepared test specimens (a) MRE beam (b) Honeycomb beam (c) MRE-honeycomb beam (d) MRE-honeycomb-MRE beam.

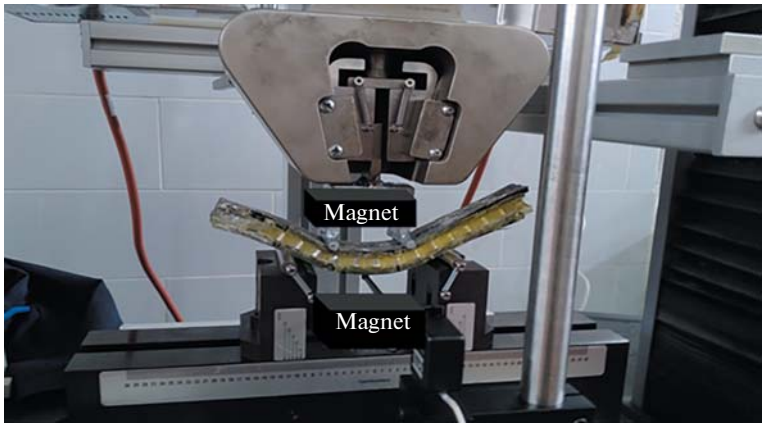

Fig. 6. Experimental set-up for the 4-point bending test.

3.4. Analyses and discussion

Figs. 8 and 9 represent the evolution of the load as a function of the deflection for the four types of sandwich hybrid beams without and with intensity of the magnetic field. The analysis of these results shows that the mechanical behavior of the sandwich materials depends on the magnetic field intensity, the MRE core and the honeycomb core.

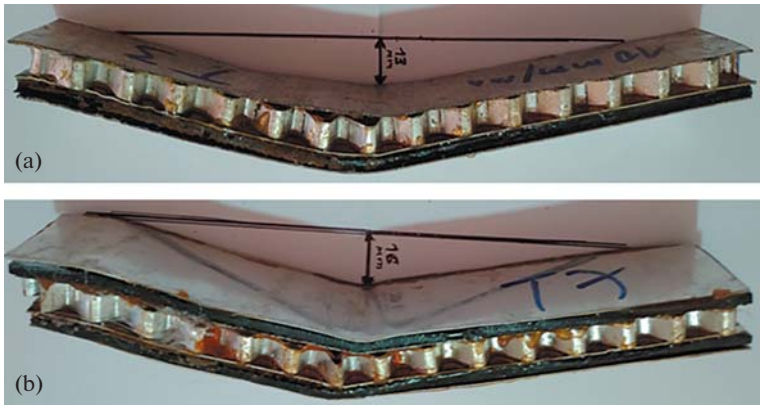

Fig. 7. Samples of sandwich beam damaged during the four-point bending test (a) MRE-Honeycomb (b) MRE-Honeycomb-MRE.

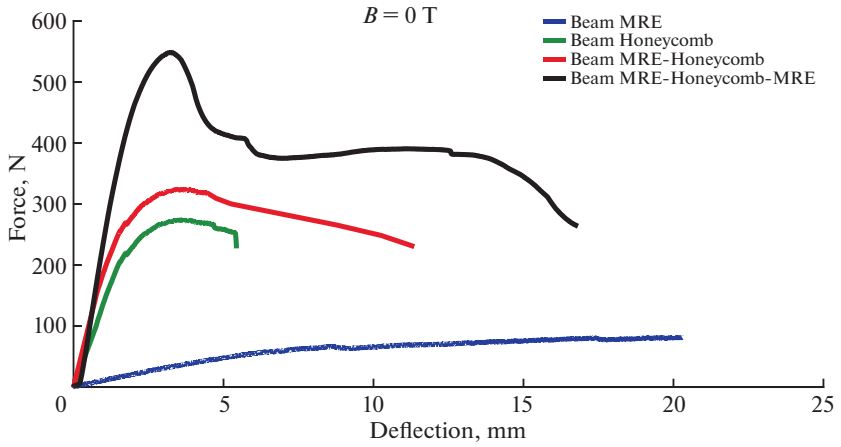

Fig. 8. Four-point bending of four specimens produced without magnetic field intensity ($B = 0$ T).

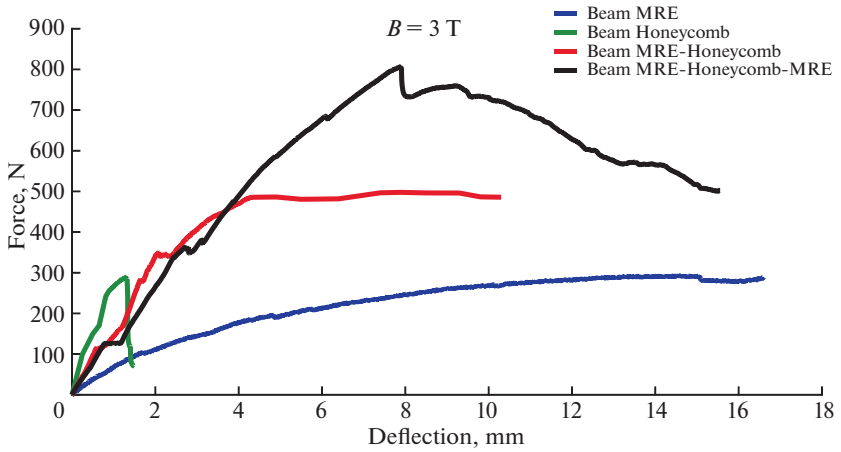

Fig. 9. Four-point bending of four specimens with magnetic field intensity of $B = 0.3$ T.

The overall behavior of MRE-Honeycomb sandwich beams in tension by bending is illustrated in Figs. 8 and 9. Indeed, these figures can be divided into three zones. The first zone presents the linear elastic behavior where none of the constituent materials of the composite is damaged, the rigidity is entirely a function of the MRE and Honeycomb. When the tensile strength of the honeycomb part is reached, the first crack appears, this area corresponds to the formation of cracks. When the crack formation is stable, the cracks open, the stiffness of the composite increases significantly compared to the second zone. The third zone corresponds to the post-peak behavior associated with the localized failure of the composite when the MRE core reaches the limit resistance. The sliding between the aluminum skins and the MRE core (tearing behavior) is observed in this area.

In the case of MRE beam, it can be seen that this structure has a very high breaking limit of more than 20 mm. Thus, it can be noted that the mechanical resistance increases with the application of a magnetic field. It can be seen that the maximum force without the application of the magnetic field is of the order of 81N, on the other hand, in the case of the application of a magnetic field intensity of 0.3T, the maximum force reaches the value of 292N, that is to say an increase of almost 300%.

In the case of the single-layer MRE-honeycomb beam, we note that this structure has a high breaking limit of more than 10 mm with a high maximum applied force. It is noted that the maximum force without the application of the magnetic field is of the order of 318N, on the other hand, in the case of the application of a magnetic field intensity of 0.3T, the maximum force reaches the value of 498N, that is to say an increase of more than 150%.

Table 4. Properties of the aluminium skins

ρ_s, kg/m^3	E_s, MPa	ν_s	h_s, mm	L_s, mm	b_s, mm
2800	72000	0.33	1	200	30

Table 5. Properties of the MRE

ρ_{MRE}, kg/m^3	E_{MRE}, MPa	ν_{MRE}	h_{MRE}, mm	L_{MRE}, mm	b_{MRE}, mm
1100	1.7	0.45	2	200	30

In the case of the double layer MRE honeycomb beam, it is noted that this structure has a very high breaking limit of more than 316 mm with a very high maximum applied force. It can be seen that the maximum force without the application of the magnetic field is of the order of 550N, on the other hand, in the case of the application of a magnetic field intensity of 0.3T, the maximum force reaches the value of 806N, that is to say an increase of more than 146%.

We note from all the static tests carried out on the four different types of test specimens (Fig. 5), it is found that the hybrid specimens are the most reliable in terms of rigidity-damping and which have better mechanical resistance due to the honeycomb layer and good resistance to rupture due to the MRE layer (strength until the rupture of the MRE layer).

4. NUMERICAL SIMULATION AND VALIDATION OF RESULTS

To assess the accuracy and efficiency of the finite element numerical simulation, we perform three types of calculations: 1) modeling of the honeycomb core by Abaqus shell elements with a very fine mesh to describe the complex geometry of the honeycomb; 2) modeling of the MRE by Abaqus solid elements with the viscoelastic material properties; 3) modeling of the skins by Abaqus solid elements with the elastic solid properties.

To validate the results of our simulation, we take the same material and geometric data of the MRE, honeycomb and skins used in the experimental part.

The mechanical and geometric properties of the skins are given in Table 4.

The mechanical and geometric properties of the MRE are given in Table 5.

The magnetorheological elastomer is identified using Abaqus by the five-terms generalized Maxwell model (Fig. 10). In this study, we used a five-term Prony series. The characteristics of the MRE determined experimentally by the DMA are given in the Table 2.

The parameters of the Prony series are given as follows:

$$g_i = \frac{G_i}{G_0 + \sum_{i=1}^{n} G_i} \tag{4.5}$$

$$\tau_i = \frac{G_i}{\eta_i} \tag{4.6}$$

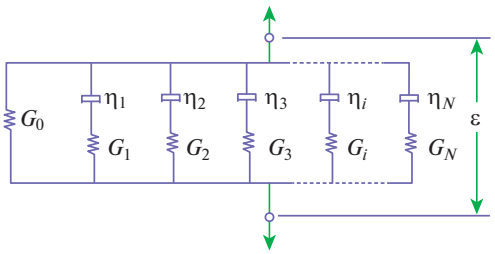

Fig. 10. Generalized Maxwell model.

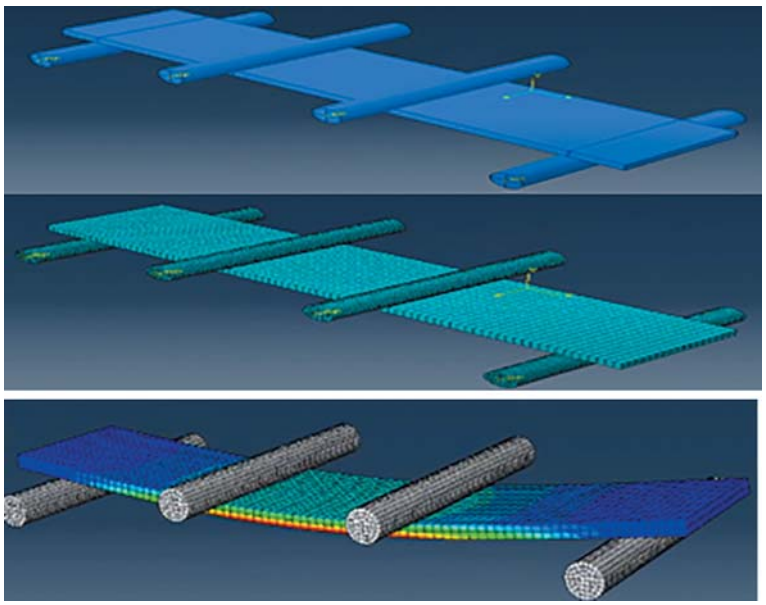

Fig. 11. Four-point bending of structure modeled by Abaqus and boundary conditions.

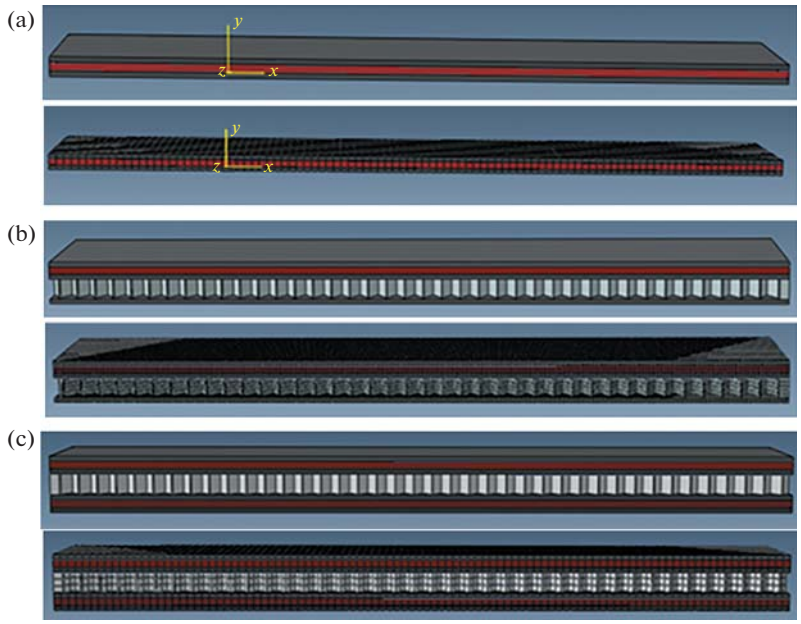

Fig 12. Different beams studied (a) MRE (b) MRE-honeycomb (c) MRE-honeycomb-MRE.

The mechanical and geometric properties of the honeycomb are given in Table 3.

In the numerical part of this present work, we studied a similar case with the experimental part, that is to say we studied the case of a four-point bending of a beam resting on two simple supports ($UX = UY = UZ = URY = URZ = 0$) and subjected to a load (Fig. 11).

To model the bending behavior of the various beams studied, a second-order C3D8R 3D solid element is used to discretize the skin and the core in MRE. A first-order S8R shell element is used to discretize the honeycomb part.

The various simulated beams and their mesh are given by Fig. 12 (a-c).

The evolution of the maximum deflection according to the mesh size is shown in Fig. 13. The results of the successive calculations are converged with a mesh size of 0.2 mm in length of the MRE and the alu-

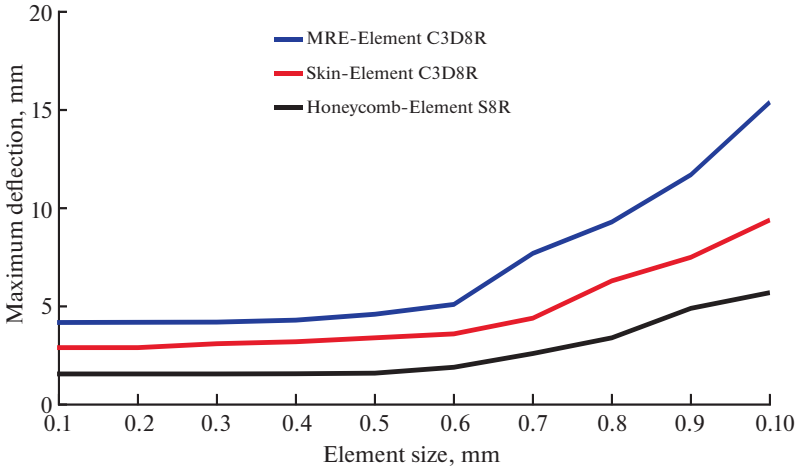

Fig. 13. Mesh convergence.

minum skin. Convergence is obtained with a mesh size of 0.4 mm honeycomb length. We also note that the sensitivity study highlights the increase in the maximum deflection with the decrease in the size of the elements. We can then say that the deflection has converged in the case of the MRE and the aluminum skin for an element value of $0.2 \times 0.2 \times 0.2$ m^3, and is converged in the case of honeycomb for an element value of 0.4×0.4 m^2, these element sizes will be used in our work.

The essential, natural boundary conditions and the displacement and rotation boundary conditions are summarized in Tables 6 and 7.

4.1. Validation of results and interpretation

The numerical simulation by finite elements of the static behavior in four-point bending of the hybrid sandwich beams in MRE-honeycomb (Fig. 12) was carried out by Abaqus software. The results in the form of transverse force-deflection curves are summarized in Figs 14 and 15 for each beam model.

The results obtained experimentally are compared with those obtained by numerical simulation using Abaqus software. The finite element calculation was carried out taking into account the variation of the mechanical properties of the MRE according to the magnetic field. The analysis of the results obtained globally shows that the mechanical resistance increases by the application of a magnetic field. This increase is due to the increase in the rigidity of the MRE which is the direct consequence of the creation of interactions between iron particles and the development of ferromagnetic pseudo-fibers.

Figs. 14 and 15 present the results of the four-point bending test carried out on MRE, Honeycomb beams and on hybrid MRE-Honeycomb beams. It can be seen that the MRE beam has a very high breaking limit corresponding to more than 20 mm with a low maximum applied force of 95 N for the case of an isotropic MRE and a significant maximum force of 286N for the case of an anisotropic MRE, which shows the effect of the magnetic field on the stiffness of the MRE. These magnetorheological elastomers are new promising smart materials with adjustable stiffness and damping by the application of a magnetic field. This effect is more notable for the case of MRE-Honeycomb beams, we observe a low breaking limit corresponding to more than 7 mm with a maximum applied force of 553N for the case of an isotropic MRE, and a maximum applied force of 810N for the case of an anisotropic MRE, which shows the double effect of MRE and Honeycomb on the rigidity of this type of structures.

Table 6. Boundary conditions

Degree of freedom	Essential	Natural
Transverse	w_y	Shear force
Rotation	θ_z	Moment
Slip	Δ_i	Normal fore

Table 7. Boundary conditions in displacement and rotation

simple – simple boundary condition	$w = 0$ $\frac{\partial^2 w}{\partial x^2}$

Table 8. Comparison between experimental results and numerical simulation

Maximum force (N) – $B = 0$ T								
MRE Beam			MRE-Honeycomb Beam			MRE-Honeycomb-MRE Beam		
Exp.	Simul.	Δ%	Exp.	Simul.	Δ%	Exp.	Simul.	Δ%
81	83	2%	318	333	4%	550	544	1%
Maximum force (N) – $B = 0.3$ T								
MRE Beam			MRE-Honeycomb Beam			MRE-Honeycomb-MRE Beam		
Exp.	Simul.	Δ%	Exp.	Simul.	Δ%	Exp.	Simul.	Δ%
292	281	4%	498	508	2%	806	730	10%

Figs. 16 and 17 represent the deflection of the three beams (MRE, MRE-honeycomb and MRE-honeycomb-MRE) obtained by numerical simulation using the Abaqus software without and with magnetic field.

Table 8 shows the values of the maximum force obtained experimentally and those obtained by numerical simulation as well as the deviations. The difference between the experimental values and those obtained by numerical simulation does not exceed 4% in the case where the magnetic field is zero, while this difference can reach 10% for the case where the magnetic field int ensity is equal 0.3 T.

Table 9 shows the values of the maximum deflection obtained experimentally and those obtained by numerical simulation as well as the deviations. The difference between the experimental values and those obtained by numerical simulation does not exceed 10% in the case where the magnetic field is zero, while this difference can reach 11% for the case where the magnetic field intensity is equal 0.3T.

In the numerical part of this article, we studied the variation of the stresses according to the strains for each case of beam. Fig. 18 shows the curve of this variation in four-point bending test simulated by Abaqus software, a nonlinear behavior is observed in the case of beams having a magnetorheological elastomer layer, this nonlinear behavior of the elastomers is due to the effect of the magnetic field [23] and it can also be linked to viscoelastic models of the stress-strain function σ(ε) [24, 25]. On the other hand, the honey-

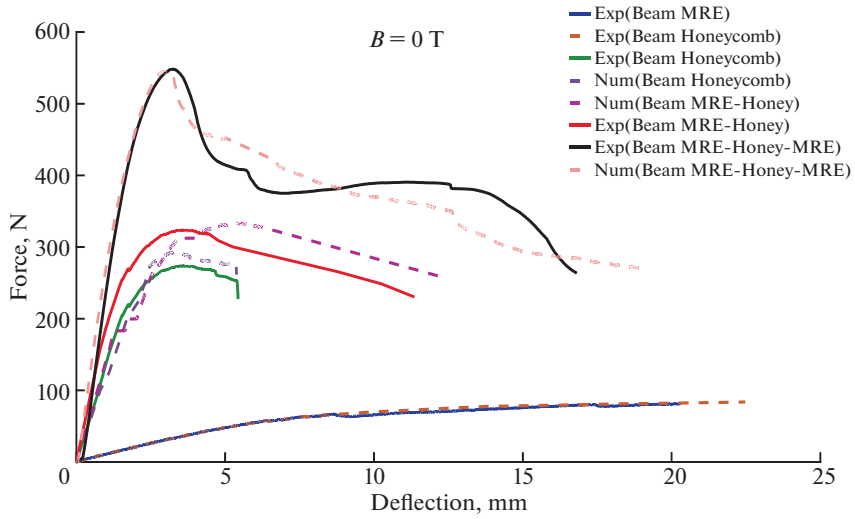

Fig. 14. Comparative analysis of experimental results and numerical simulation, without magnetic field.

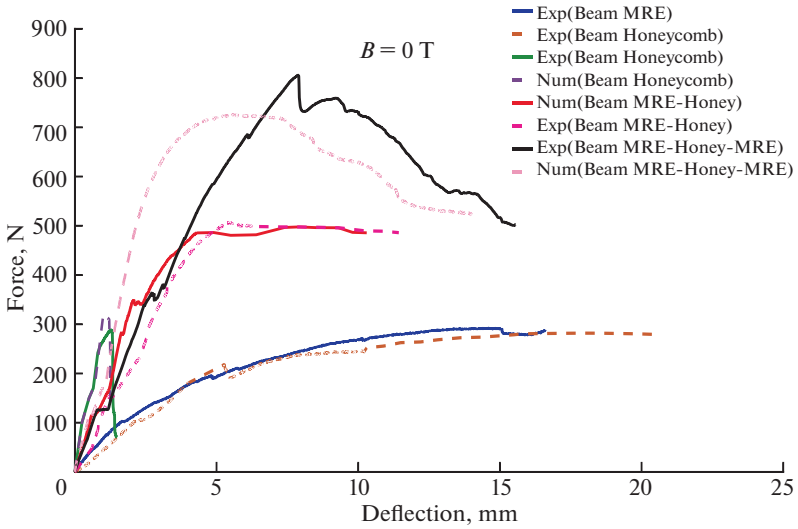

Fig. 15. Comparative analysis of experimental results and numerical simulation, with magnetic field.

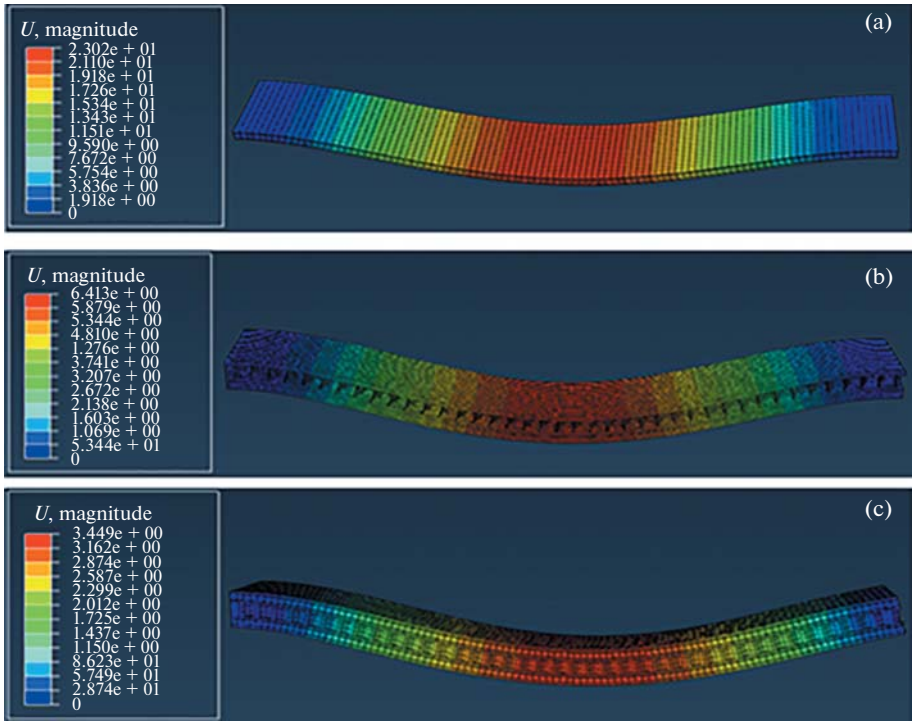

Fig. 16. Simulation results of different beams studied without magnetic field ($B = 0$ T) (a) MRE (b) MRE-honeycomb (c) MRE-honeycomb-MRE.

comb beam shows a linear behavior of an elastic solid [26]. Therefore, the bending curve (Fig. 18) shows a considerable nonlinear increase in stress as a function of strain for the case of MRE-Honeycomb hybrid beams.

The results of the simulation and the deformation modes are illustrated in Fig. 19.

The results obtained by numerical simulation and experimental tests are in good agreement, for the four types of elaborated sandwich beams. The difference found between the experimental results and numerical simulation still remains acceptable and can be attributed to the real conditions of contact at the

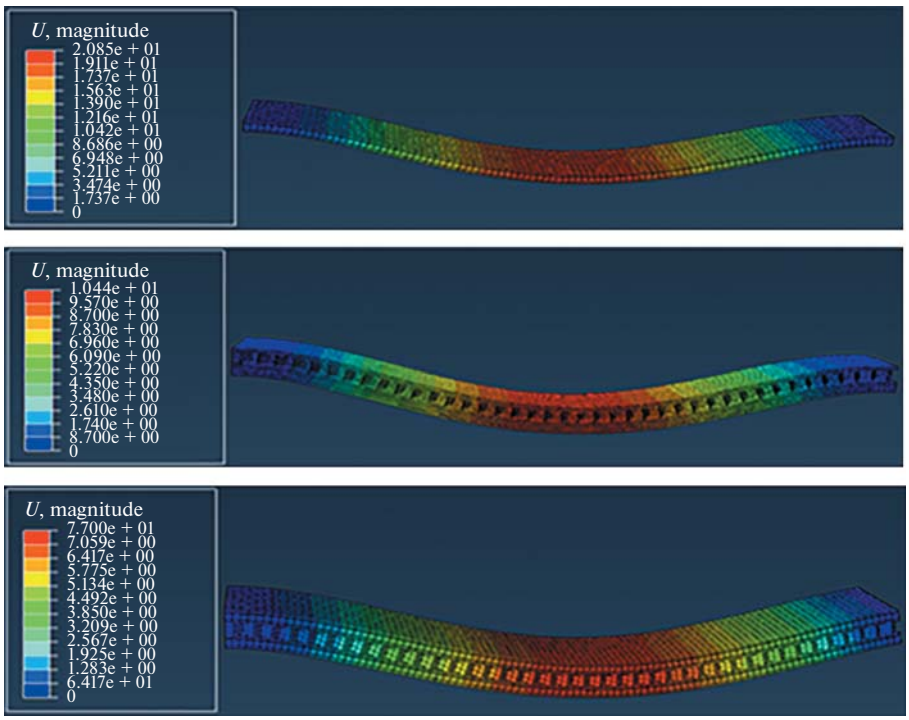

Fig. 17. Simulation results of different beams studied with magnetic field ($B = 0.3$ T) (a) MRE (b) MRE-honeycomb (c) MRE-honeycomb-MRE.

surfaces between different layers, whose calculation by numerical simulation did not take into account these exact real conditions.

5. CONCLUSIONS

The use of magnetorheological elastomer makes it possible to significantly improve the qualitative and quantitative behavior of the honeycomb specimens. The reinforced specimens present three phases of behavior, and there is a significant increase in mechanical resistance, between 150–300% for the ultimate load depending on the configuration of the specimens produced.

Honeycomb specimens reinforced with one layer or two layers of MRE subjected to a magnetic field intensity present better resistance and better rigidity than those tested without the effect of the magnetic field.

Depending on the configuration of the developed specimens, the ultimate load of the honeycomb-MRE specimens exposed to a magnetic field intensity is higher compared to those tested without the effect of the magnetic field, which can be explained by an increased rigidity, which leads to reduce the appearance of cracks.

Table 9. Comparison between experimental results and numerical simulation

Maximum deflection (mm)– $B = 0$ T								
MRE Beam			MRE-Honeycomb Beam			MRE-Honeycomb-MRE Beam		
Exp.	Simul.	Δ%	Exp.	Simul.	Δ%	Exp.	Simul.	Δ%
21.10	23.02	09%	05.81	06.40	10%	03.43	03.45	0.5%
Maximum deflection (N) – $B = 0.3$ T								
MRE Beam			MRE-Honeycomb Beam			MRE-Honeycomb-MRE Beam		
Exp.	Simul.	Δ%	Exp.	Simul.	Δ%	Exp.	Simul.	Δ%
18.09	20.08	11%	10.03	10.44	4%	08.18	07.70	6%

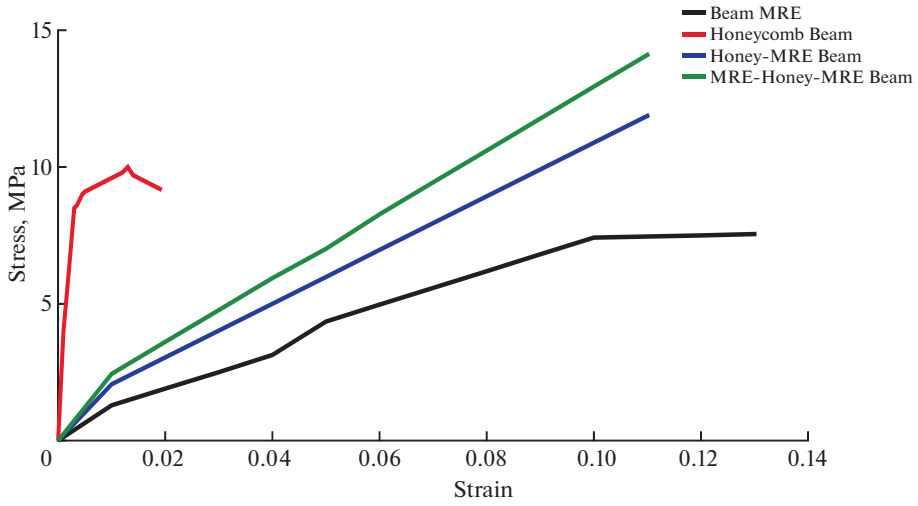

Fig. 18. Stress-strain variation of different cases.

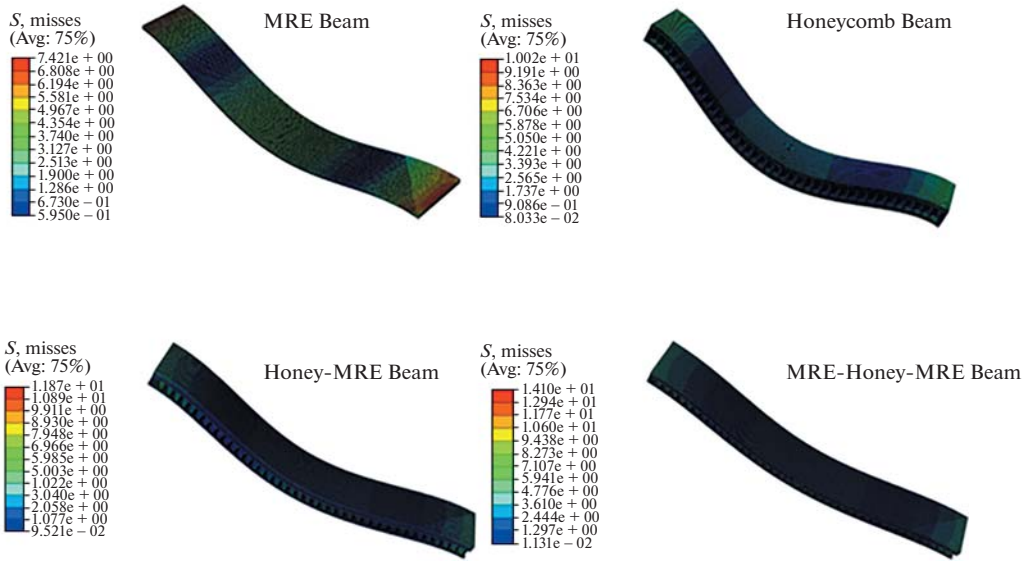

Fig. 19. Modes of deformations for different cases.

The results of the experimental analysis and numerical simulation of the behavior of smart hybrid sandwich structures made of honeycomb magnetorheological elastomer showed an excellent performance of mechanical resistance against failure thanks to the MRE core and the honeycomb structure. This technique offers engineers essential solutions to reduce failure and which influences the increase in the lifespan of mechanical structures (compressor blades, aircraft wings, rotor blades, etc.).

FUNDING

No funding was received.

CONFLICT OF INTEREST

@@@@@@@

REFERENCES

1. A. Jamal, S. Yves, P. J-Lu, et al., "Numerical simulation and experimental bending behaviour of multi-layer sandwich structures," J. Theor. Appl. Mech. **52** (2), 431–442 (2014).
2. K. B. Anil and H. Mokarram, "A review on magneto-mechanical characterizations of magnetorheological elastomers," Compos. Part B: Eng. **200**, 108348 (2020). https://doi.org/10.1016/j.compositesb.2020.108348
3. C. B. Fevzi and S. Selim, "Active vibration suppression of elastic blade structure: Using a novel magnetorheological layer patch," J. Intell. Mater. Syst. Struct. **29** (19), 3792–3803 (2018). https://doi.org/10.1177/1045389X18799441
4. S. Bornassi, H. M. Navazi, and H. Haddadpour, "Coupled bending-torsion flutter investigation of MRE tapered sandwich blades in a turbomachinery cascade," Thin-Walled Struct. **152**, 106756 (2020). https://doi.org/10.1016/j.tws.2020.106765
5. B. Luca, P. Fulvio, C. Stefano, et al., "Manufacturing, and characterization of hybrid carbon/hemp sandwich panels," J. Mater. Eng. Perform. **31**, 769–785 (2022). https://doi.org/10.1007/s11665-021-06186-1
6. K. R. Sanjay, S. Bamadev, R. N. Nayak, et al., "Nonlinear analysis of a viscoelastic beam moving with variable axial tension and time-dependent speed," Iran. J. Sci. Technol. Tran. Mech. Eng. **48**, 411–434 (2024). https://doi.org/10.1007/s40997-023-00666-6
7. M. A. Moreno-Mateos, K. Danas, and D. Garcia-Gonzalez, "Influence of magnetic boundary conditions on the quantitative modelling of magnetorheological elastomers," Mech. Mater. **184**, 104742 (2023). https://doi.org/10.1016/j.mechmat.2023.104742
8. B. Hou, S. Pattofatto, Y. L. Li, et al., "Impact behavior of honeycombs under combined shear-compression. Part I: Experiments," Int. J. Solids Struct. **48** (5), 687–697 (2011). https://doi.org/10.1016/j.ijsolstr.2010.11.005
9. B. Hou, H. Zhao, S. Pattofatto, et al., "Inertia effects on the progressive crushing of aluminium honeycombs under impact loading," Int. J. Solids Struct. **49** (19–20), 2754–2762 (2012). https://doi.org/10.1016/j.ijsolstr.2012.05.005
10. M. R. Rokn-Abadi, P. Shahali, and H. R. Haddadpour, "Effects of magnetoelastic loads on free vibration characteristics of the magnetorheological-based sandwich beam," J. Intell. Mat. Syst. Struct. **31** (7), 1015–1028 (2020). https://doi.org/10.1177/1045389X20905986
11. L. Guenfoud, N. Chikh, S. Aguib, et al., "Experimental analysis and numerical simulation of the behavior of smart sandwich beams in magnetorheological elastomer–honeycomb," J. Brazil. Soc. Mech. Sci. Eng. **45**, 538 (2023). https://doi.org/10.1007/s40430-023-04452-y
12. U. Sharif, B. Sun, S. Hussain, et al., "Dynamic behavior of sandwich structures with magnetorheological elastomer : a review," Materials **14** (22), 7025 (2021). https://doi.org/10.3390/ma14227025
13. F. de Souza Eloy, G. Ferreira Gomes, A. C. Ancelotti Jr., et al., "Experimental dynamic analysis of composite sandwich beams with magnetorheological honeycomb core," Eng. Struct. **176**, 231–242 (2018). https://doi.org/10.1016/j.engstruct.2018.08.101
14. M. Tourab and S. Aguib, "Experimental analysis of the thermal effect of the magneto mechanical behavior of viscoelastic elastomer," J. Adv. Res. Fluid Mech. Therm. Sci. **53** (1), 25–34 (2019).
15. H. Zniker, I. Feddal, B. Ouaki, et al., "Experimental and numerical investigation of mechanical behavior and failure mechanisms of PVC foam sandwich and GRP laminated composites under three-point bending loading," J. Fail. Anal. Prevent. **23**, 66–78 (2023). https://doi.org/10.1007/s11668-023-01596-w
16. A. Sharma, V. C. Khan, G. Balaganesan, et al., "Performance of nano-filler reinforced composite overwrap system to repair damaged pipelines subjected to quasi-static and impact loading," J. Fail. Anal. Prevent. **20**, 2017–2028 (2020). https://doi.org/10.1007/s11668-020-01013-6
17. J. Liu, Z. Xi, and J. Zhao, "Failure characteristics of the active-passive damping in the functionally graded piezoelectric layers-magnetorheological elastomer sandwich structure," Int. J. Mech. Sci. **215**, 106944 (2022). https://doi.org/10.1016/j.ijmecsci.2021.106944
18. A.T. Settet, S. Aguib, A. Nour, et al., "Study and analysis of the magneto-mechanical behavior of smart composite sandwich beam in elastomer," Mechanika **25**, 320–325 (2019). https://doi.org/10.5755/j01.mech.25.4.22713
19. S. Timoshenko and S. Woinowsky-Krieger, *Theory of Plates and Shells* (Mcgraw-Hill College, New York, 1959).
20. E. J. Barbero, *Introduction to Composite Materials Design*, 2nd ed. (CRC Press, 2010).
21. L. C. Bank, *Composites for Construction: Structural Design with FRP Materials* (John Wiley & Sons, 2006).

22. C. Astm, "1018, Standard test method for flexural toughness and first crack strength of fibre reinforced concrete (Using beam with third-point loading)," in *American Society of Testing and Materials, Annual Book of Standard,* Vol. 4 (ASTM, Philadelphia, 1994), pp. 02509–02516.
23. S. Lucarini, M. Hossain, and D. Garcia-Gonzalez, "Recent advances in hard-magnetic soft composites: Synthesis, characterisation, computational modelling, and applications," Compos. Struct. **279**, 114800, (2022). https://doi.org/10.1016/j.compstruct.2021.114800
24. J. Kolařík and A. Pegoretti, "Non-linear tensile creep of polypropylene: Time-strain superposition and creep prediction," Polymer **47** (11), 346–356 (2006). https://doi.org/10.1016/j.polymer.2005.11.013
25. W. M. Madigosky and G. F. Lee, "Improved resonance technique for materials characterization," J. Acoust. Soc. Am. **73** (14), 1374–1377 (1983). https://doi.org/10.1121/1.389242
26. N. Wang and Q. Deng, "Efect of axial deformation on elastic properties of irregular honeycomb structure, " Chin. J. Mech. Eng. **34**, 51 (2021). https://doi.org/10.1186/s10033-021-00574-3

SPELL; OK